Understanding Amorphization Mechanisms Using Ion Irradiation in-situ within a TEM and 3D Damage Reconstruction

Osmane Camara*, Matheus A. Tunes, Graeme Greaves, Anamul H.Mir, Stephen Donnelly and Jonathan A. Hinks

School of Computing and Engineering, University of Huddersfield, Queensgate, Huddersfield, HD1 3DH, United Kingdom

Abstract

In this work, ion irradiations in-situ of a transmission electron microscope are performed on single-crystal germanium specimens with either xenon, krypton, argon, neon or helium. Using analysis of selected area diffraction patterns and a custom implementation of the Stopping and Range of Ions in Matter (SRIM) within MATLAB (which allows both the 3D reconstruction of the collision cascades and the calculation of the density of vacancies) the mechanisms behind amorphization are revealed. An intriguing finding regarding the threshold displacements per atom (dpa) required for amorphization results from this study: even though the heavier ions generate more displacements than lighter ions, it is observed that the threshold dpa for amorphization is lower for the krypton-irradiated specimens than for the xenon-irradiated ones. The 3D reconstructions of the collision cascades show that this counter-intuitive observation is the consequence of a heterogeneous amorphization mechanism. Furthermore, it is also shown that such a heterogeneous process occurs even for helium ions, which, on average induce only three recoils per ion in the specimen. It is revealed that at relatively high dpa, the stochastic nature of the collision cascade ensures complete amorphization via the accumulation of large clusters of defects and even amorphous zones generated by single-helium-ion strikes.

1.0 Introduction

Amorphization of silicon during ion irradiation is a matter that has been frequently addressed in the scientific literature.[1]–[9] One of the main reasons behind the interest in this topic is that silicon, which has been the primary material used in the semiconductor industry over the past 60 years, is routinely modified via ion beam processing.[10] However, Germanium is now being considered for future use in transistor devices mainly due to its higher charge carrier mobility compared to silicon.[11] It also is a remarkable material for optoelectronics where there is currently a growing interest regarding its ability to behave as a direct band-gap semiconductor when subjected to strain and heavy doping.[12]

By implanting ions into a semiconductor, its electronic properties can be tuned.[13], [14] However, the formation of defects during irradiation is a drawback of ion implantation as they may interfere with the dopants, create extended defects and even lead to amorphization.[15]–[17] Yet, amorphization can also be beneficial as channelling effects which occur in crystals may result in implantation profiles that are difficult to predict in crystalline materials. Therefore, ion beam doping is sometimes deliberately performed on pre-amorphized material to better control the implantation depth of dopants. Typically, the pre-amorphization step is performed using inert gas or self-ion irradiation.[18], [19]. To compare the propensity of different ions to induce amorphization, the threshold displacements per atom (dpa) for amorphization is generally used.[2], [20]. Currently, due to the miniaturisation of transistors it becomes more and more imperative to precisely control the dpa (and the fluence) for complete amorphization, the depth of the amorphous material and the presence of isolated amorphous zones, as these features greatly impact the properties of sub-micron transistors. However, controlling the formation of amorphous material at the nanoscale requires a greater understanding of the mechanisms responsible for it.

Whilst ion implantation is one of the principal techniques used to process silicon, the mechanisms which lead to amorphization are still disputed, and this especially in germanium which has been less studied over the last decades [1] There are however, key models that are regularly invoked in the literature: the

homogeneous or heterogeneous amorphization models and combinations thereof .[1]–[3], [5], [17], [21]–[25]

The homogeneous model considers amorphization to occur abruptly when the density of defects reaches a certain threshold value. Once this threshold is reached, it becomes energetically favourable to be in an amorphous state rather than in a highly-defective crystalline phase and thus the crystal structure collapses into its amorphous phase.[17], [21] However, evidence of amorphous pockets within semiconductors irradiated by heavy ions seems to indicate that the homogeneous model is not applicable for heavy ion irradiation. It has therefore been proposed that, in such cases, amorphous regions (or pockets) may form directly as a result of single ion impacts and that complete amorphization then results from their accumulation.[1], [2] Whilst this model may be appropriate for heavy ions, the lighter the ion used for irradiation the less likely it is to produce amorphous regions in single impacts. [1], [26] For this reason, a modified version of the heterogeneous model has been introduced where, instead of an amorphous region produced directly by a single ion impact, such a region could be the result of the overlap of damaged regions that result from single ion impacts.[22] The average number of overlaps *m* needed to turn a crystalline region into an amorphous region of volume *V* has been observed to depend on the mass of the incoming ion.[2], [22]

According to this model, the evolution of the amorphous fraction, f_a , as a function of the ions per unit volume dose, *D*, follows the equation (1) proposed by Gibbons:[2], [22]

$$f_a = 1 - \sum_{k=0}^{m} \frac{(V.D)^k}{k!} e^{-V.D} \qquad (1)$$

Furthermore, as illustrated by figure 1(a) it has been proposed that an ion may, via a single impact, produce an amorphous region of volume V_α surrounded by a highly damaged region of volume V_d which is still crystalline but can become amorphous after *m* overlaps.[25] In this case the total volume *V* which will become amorphous is equal to $V_\alpha + V_d$ where V_d is approximated as being the volume which

becomes amorphous after one overlap (m = 1) and where f_a is given by equation (2).[25] (Obviously, if V_α = 0, equation(2) is equivalent to equation (1)).

$$f_a = 1 - e^{-V_\alpha . D} e^{-V_d . D} (1 + \sum_{k=0}^{m} \frac{(V_d . D)^k}{k!}) \qquad (2)$$

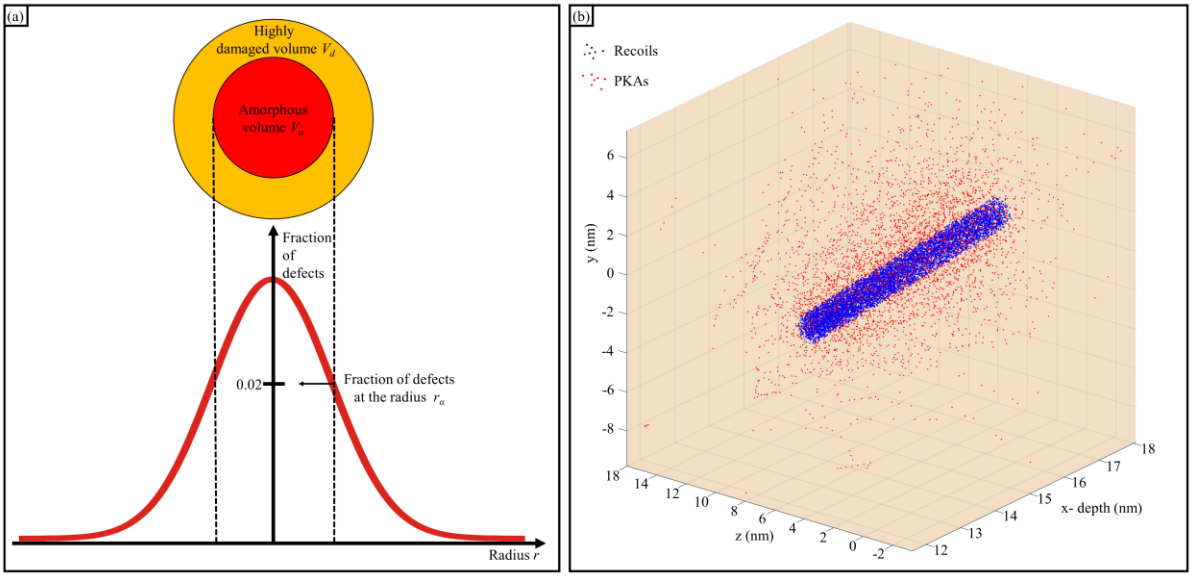

Figure 1. *(a) Schematic showing an amorphous volume V_α surrounded by a shell of damaged crystal of volume V_d.(b) Example showing in the 3D plot representing an inner section (at depth x) of the germanium specimen , the recoils within V_α due to irradiation with a 300 keV xenon ion beam. The recoils within V_α are shown in blue and the primary knock-on atoms (PKA) within and outside V_α are shown in red. The 3D plots is shown after bombardment by 1000 xenon ions and V_α=108 nm^3.*

As these four models differ, the evolution of the f_a during ion irradiation also differs and can be depicted for a given material by the examples in figure 2 that shows for each model, f_a as a function of the fluence, where in all cases the material is considered amorphous at the same fluence and where the values of V are similar.

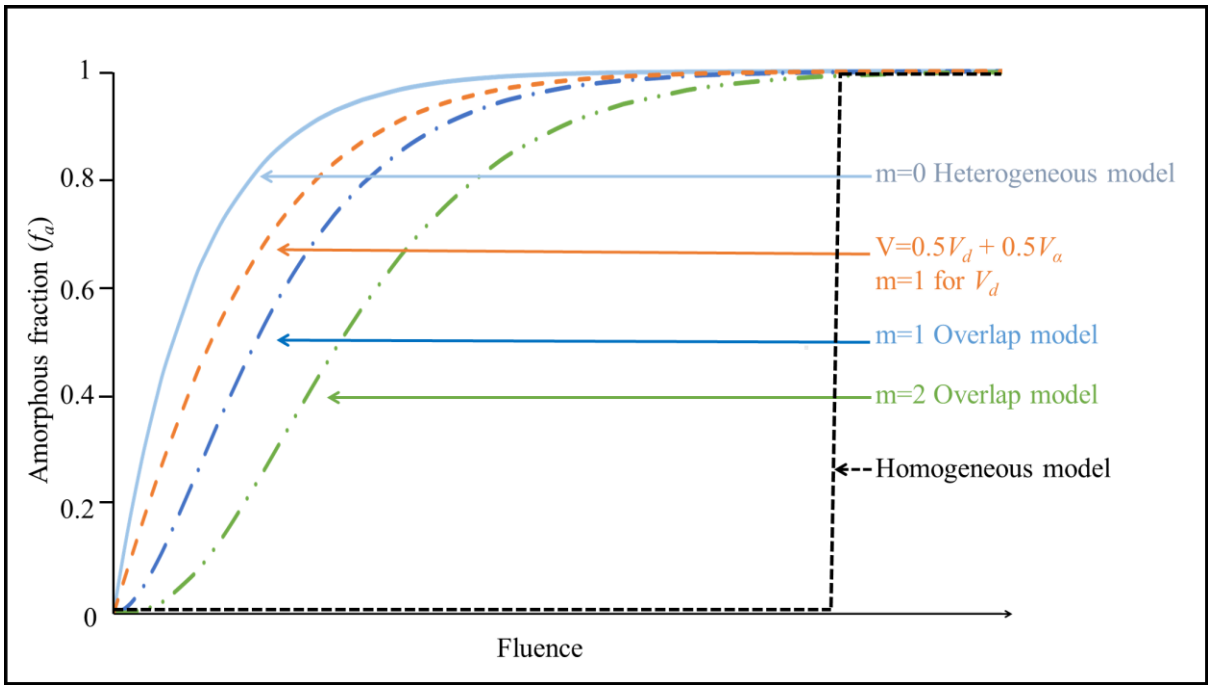

Figure 2. *Schematic showing the expected evolution of the amorphous fraction depending on the proposed models for amorphization and where complete amorphization occurs at the same fluence. For all models except the homogeneous model the volume V responsible for the build-up of amorphous material is the same.*

In the present work, we have focused on the amorphization of single crystal germanium specimens. These are irradiated *in situ* within a transmission electron microscope (TEM) using various inert gases (helium, neon, argon, krypton and xenon) whilst the evolution of the selected area diffraction pattern (SADP) is monitored. Via a correlation between the experimental results and equation (2), for each case V and m are calculated and an implementation of the Monte-Carlo (MC) software *Stopping and Range of Ions in Matter* (SRIM) within MATLAB is used to explore the three dimensional collision cascade morphology and to determine V_α based on the density of vacancies generated during irradiation.[27] As the energy regime is chosen to allow the ions to pass through the specimens for all irradiations conditions, the volumes V, V_α and V_d are approximated as cylindrical volumes centred along the ion direction as in previous work based on the overlap model and this is illustrated in the example in figure

1(b) where the recoils within V_α are indicated by blue data points.[22] (The MatLab script used in this work to generate the 3D plots and determine the vacancies densities is available upon request).

This work unravels the mechanisms behind amorphization and how the mass of the ions affects it. It shows that only the heterogeneous model can explain the experimental results presented herein, which, indicate that a lighter ion can induce amorphization at a lower or similar dpa than a heavier ion. It is also shown that at a sufficiently high dpa, the stochastic nature of the collision cascades enables helium ions (which in this work induce on average only 3 recoils) to induce amorphization via an agglomeration of clusters of defects or even amorphous regions, thus via one of the three heterogeneous mechanisms described above.

Furthermore, this work provides a robust set of data that allows an estimation of the fluences, the ions per unit volume (D) or displacement per atom (dpa) for amorphization when irradiation is performed with ions whose atomic masses range from 4 amu (helium) to 132 amu (xenon).

2.0 Experimental details

Single crystal germanium (111)-oriented TEM samples were mechanically polished and subsequently thinned to electron transparency by means of a Gatan precision ion polishing system (PIPS). Thicknesses were determined using the TEM operated in energy-filtered TEM (EFTEM) mode via a routinely used technique which has been described elsewhere and were found to be in the range of 20–30 nm.[28] The specimens irradiated with xenon, krypton, argon, neon and helium ions had thicknesses of 30 nm, 23 nm, 19 nm, 23 nm and 23 nm, respectively.

Samples were irradiated at room temperature with either xenon, krypton, argon, neon or helium ions at energies chosen such that the range of the ions within the sample are relatively close (except for the helium irradiation case) equivalent and more importantly such as the range is substantially larger than the specimen thickness as usually required when using equation 1 or 2 (300, 200, 100, 80 and 70 keV, respectively)[25], [29]. Furthermore, the average damage rate was the same for all irradiation cases, corresponding to approximately 4.5×10^{-4} dpa/s which was chosen as to be low enough to monitor the amorphization build-up at each irradiation step. The irradiations were performed *in situ* within a TEM

at the Microscopes and Ion Accelerators for Materials Investigations (MIAMI) facility using the MIAMI-2 system which comprises a Hitachi H-9500 TEM equipped with a Gatan OneView digital camera with 16 mega-pixels coupled with a 350 kV ion accelerator. The samples were irradiated at 18.7° from the [111] direction thus avoiding ion beam channelling effects.

The samples were tilted such that the electron beam was incident along the [111] zone axis for SADP acquisition. The degree of crystallinity was thus monitored at each irradiation step via the SADP. As electron beams are known to retard or prevent amorphization,[30], [31], the electron beam was not incident on the sample during ion irradiation steps and the samples were only exposed to it during SADP acquisition. The condenser lens settings and selected area of the sample were kept constant throughout each experiment to ensure direct comparability between the SADPs.

The evolution of the amorphous fraction, f_a, during ion bombardment was measured on the SADP raw data using the radial density function in the image processing program, ImageJ, to monitor the intensity of the amorphous rings.[32] At full amorphization (when diffraction spots were no longer visible), the intensity of the Debye-Scherrer rings (which is directly proportional to the amount of amorphous material) corresponds to $f_a = 1$.[2] After background noise subtraction via the software Origin, the evolution of f_a was then used to determine V and m via fitting with equation (2). The selected area of the sample was considered to be fully amorphous when no diffraction spots were detectable in the SADP and the threshold dpa was thus calculated from the amorphization fluence using SRIM.

In order to model the ion-induced atomic collision cascades in 3D, a modified version of the open-source *Ion Damage and RAnge in the Geometry Of Nanowires* (IDRAGON) code which implements SRIM within MATLAB has been used.[33] Version 2013 of SRIM was run in the "Detailed calculation with full damage cascades" for 1 ion at a time using a displacement energy of 21 eV.[34] The collision cascade calculated by SRIM (in the collision.txt file) was then imported into MATLAB where the number of recoils was calculated within successive cylindrical volumes of radius r_x whose axes were centred along the ion beam direction. The cylindrical volumes had depth equal to the amorphization thickness (from 19 to 30 nm depending on the irradiation conditions) and radius r_x ranging from 0.1 nm

to a radius large enough to include all the recoils generated by the ion. The 3D scanning of a collision cascade was performed for 1000 collision cascades using 1000 random seed numbers within SRIM. The displacement data output files from SRIM provide the displacements per ion as a function of depth of the target material, thus, allowing the calculation of the dpa for the thickness matching the actual size of the specimens and at the fluences used during the experiments. To calculate the dpa (via the displacement data output) and the ratio (S_e/S_n) between the electronic energy loss (S_e) and the nuclear energy loss (S_n), SRIM was run for 99999 ions under similar conditions.

3.0 Results

Using the SRIM output data and MATLAB, the recoils generated during the MC calculations can be plotted in 3D. As all recoils travel within the sample leaving behind a vacant site, each recoil induces the formation of a vacancy (except for a negligible number of replacement collisions). Consequently, as the 3D plot gives the position of each recoil, it can also be considered to show where the vacancies are generated during irradiation. Therefore, in this work the terms recoils and vacancies will be used interchangeably hereafter. In germanium, the collapse of a crystalline region into an amorphous phase has been reported by Swanson et al. to occur when the defect density reaches a minimum of 0.02 of the atomic fraction.[35] When considering that irradiation induces equal number of interstitials and vacancies (i.e. Frenkel pairs), the minimum vacancy density required must thus correspond to 0.01 of the atomic fraction. As the germanium atomic density is $\approx 4.42 \times 10^{22}$ atom.cm^{-3}, for an ion to induce such density it must generate 0.442 vacancies.nm^{-3}.ion^{-1} in a given region of the collision cascade, which can be approximated as 0.442 recoils.nm^{-3}.ion^{-1}.

As shown in the example in figure 1 using the aforementioned MATLAB script, it was possible to locate in the plot the volume V_α within which the minimum recoil concentration was equal to or greater than the threshold value, 0.442 recoils.nm^{-3}.ion^{-1}. As summarised in table 1 the formation of such a volume

V_α during irradiation is expected to occur for all cases except for the specimen bombarded with helium ions. Indeed, with this specimen the threshold value cannot be reached as the total number of recoils per ions is very low (3 recoils.ion^{-1}).

Ion	**Total number of recoils (recoils.ion^{-1})**	***M***	**V_α (nm^3)**	**V_d (nm^3)**	**Threshold dpa**	**S_e/S_n**	**Fluence at full amorphization (ions.cm^{-2})**
Xenon	1595	1	108	700	0.37±0.02	0.63	3.0×10^{13}
Krypton	768	1	55	400	0.32±0.02	0.65	4.2×10^{13}
Argon	294	1 or 2	9	45(m = 1) or 78(m = 2)	0.72±0.04	1.03	1.8×10^{14}
Neon	147	2	2	38	0.83±0.04	1.51	5.1×10^{14}
Helium	3	3	0	0.17	11.3±0.6	40.67	3.5×10^{17}

Table 1 *Total number of recoils per ion, m, V_d and V_α and the threshold dpa and fluence for amorphization for the different ions.*

During the irradiations, damage accumulation gradually led to amorphization of all the irradiated specimens at which point the SADPs showed no sign of crystalline material with only Debye-Scherrer rings detectable as shown in figure 3 for the 300 keV xenon ion irradiation. The SADP of the pristine germanium is shown in figure 3(a) and during irradiation the partially amorphous character of the irradiated specimen is revealed by the presence of both rings and spots in figure 3(b) whilst only the rings remain in figure 3(c), thus, indicating that the sample is fully amorphous.

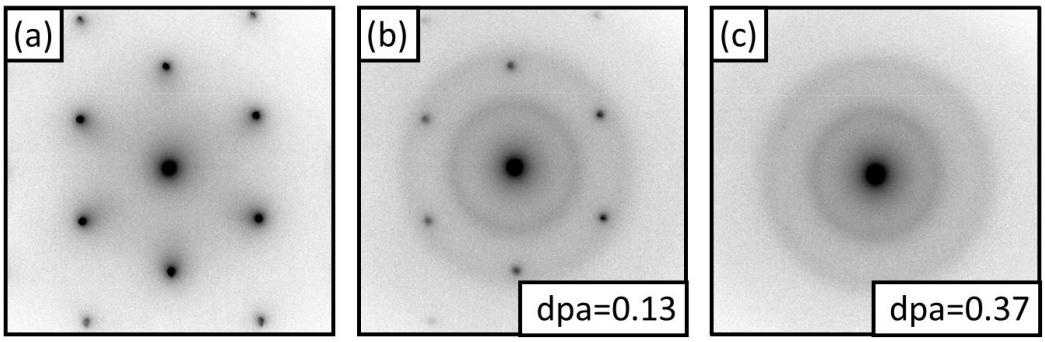

Figure 3. *Evolution of SADPs taken of germanium irradiated with 300 keV xenon at room temperature: (a) before irradiation the SADP indicates that the specimen is a single crystal; (b)the germanium is partially amorphous after irradiation with 300 keV xenon ions to a fluence of 1.3×10^{13} ions.cm^{-2} (0.13 dpa); and (c) fully amorphous at a fluence of 3.0×10^{13} ions.cm^{-2} (0.37 dpa).*

The evolution of the intensity of the amorphous rings for each irradiation is shown in figures 4 (a)-(e), (The small decrease of the intensity of the amorphous rings at the beginning of some irradiation(s) is likely due to removal of a thin layer of contamination and/or native oxide). In the figures are also shown the amorphous fraction f_a according to a fitting between the experimental results and equation (2). The experimental results are fitted with the equations via the parameters V_α, V_d, and m, where the values of V_α were previously determined via the analysis of the 3D plot and where V_α is calculated based on the theoretical threshold defect fraction for amorphization which, as shown in figure 1, has a value of 0.02. It is worth stating that in the case of the specimen irradiated by helium ions, whilst the intensity of the amorphous rings was close to saturation at 1.4×10^{17} ions.cm^{-2}, the SADP continued to exhibit crystalline spots, (thus crystallites), consequently, the irradiations was performed until amorphous rings only were detected.

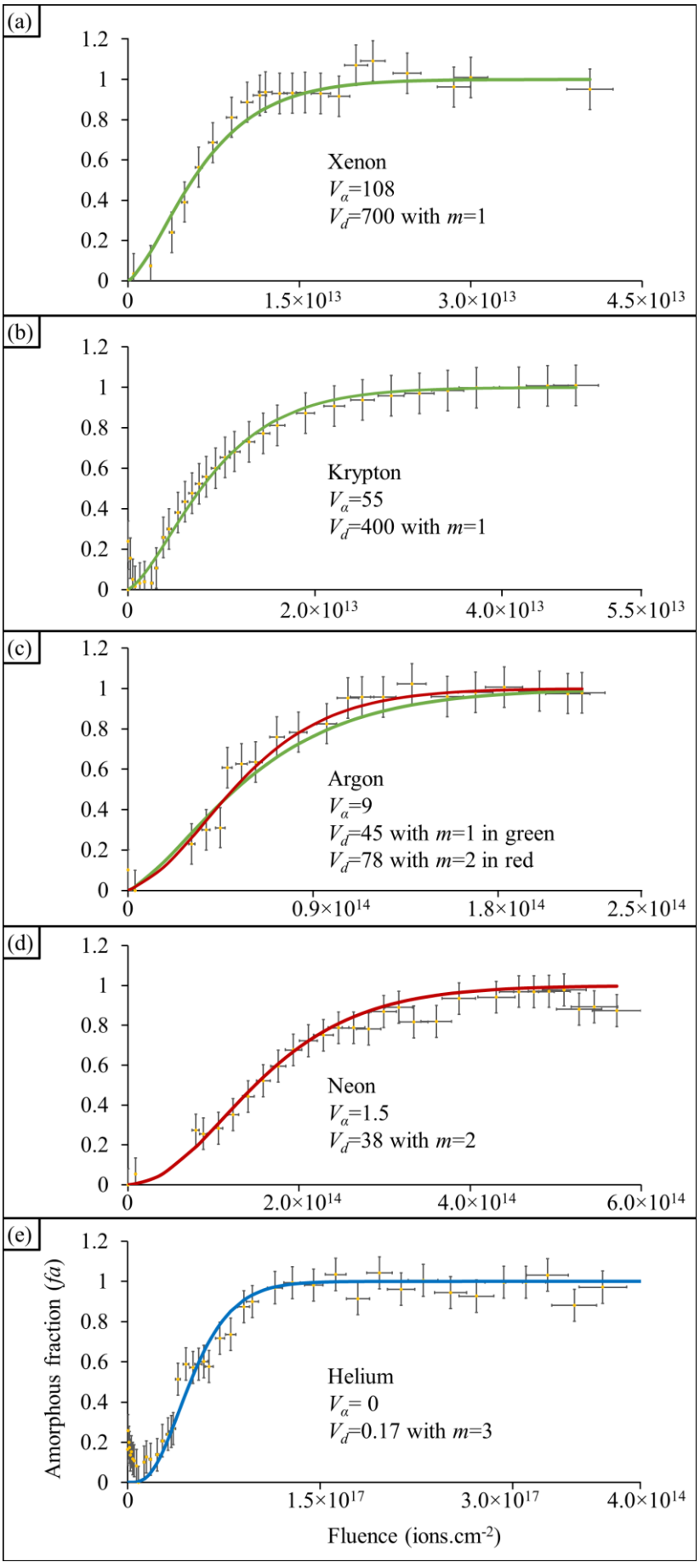
(a)
Xenon
V_α=108
V_d=700 with m=1
0
1.5×10^13
3.0×10^13
4.5×10^13
(b)
Krypton
V_α=55
V_d=400 with m=1
0
2.0×10^13
4.0×10^13
5.5×10^13
(c)
Argon
V_α=9
V_d=45 with m=1 in green
V_d=78 with m=2 in red
0
0.9×10^14
1.8×10^14
2.5×10^14
(d)
Neon
V_α=1.5
V_d=38 with m=2
0
2.0×10^14
4.0×10^14
6.0×10^14
(e)
Helium
V_α= 0
V_d=0.17 with m=3
0
1.5×10^17
3.0×10^17
4.0×10^14
Amorphous fraction (fa)
Fluence (ions.cm^{-2})
0
0.2
0.4
0.6
0.8
1
1.2

Figure 4. *Evolution of the amorphous fraction as a function of fluence during room temperature irradiation of germanium according to equation (2) (indicated by the continuous curves) and to the experimental data (indicated by the data points with error bars) with: (a) 300 keV xenon; (b) 200 keV krypton; (c) 100 keV argon; (d) 80 keV neon; and (e) 70 keV helium.*

The recoil densities were not only determined just for the volume V_α but as a function of the volume for each irradiation. The fraction of defects corresponding to these recoil densities are shown in figure 5, (except for the helium case as the overall number of recoils is an order of magnitude lower). As expected, under these experimental conditions where the ion ranges are relatively close, heavier ions give the regions with highest vacancy concentrations as their larger collision cross-sections mean that their mean-free-path between collisions is shorter,[1], [26], producing more recoils as shown in table 1. These observations illustrate the tendency of heavier ions to more readily induce highly damaged volumes V_d and amorphous regions V_α.

For each irradiation condition, the dpa at which complete amorphization was observed and the ratio (S_e/S_n) are summarised in table 1. Additionally, also shown in the table are the number of overlapping cascades, m, required to make V_d amorphous (m = 0 meaning that no overlap is required and thus amorphization is induced in a single impact) and the volume V of the amorphous regions as determined by equation 2. As previously reported, V was found to decrease whilst m and S_e/S_n were found to increase with decreasing ion mass.[2], [3], [22]

As shown in table 1, the threshold dpa at which germanium became amorphous also seems to be associated with the incident ion mass and has a tendency to be lower when the mass of the ion increases. However, there is an exception in the case of krypton for which the threshold dpa is slightly lower than that for xenon even though xenon is a much heavier ion than krypton. To verify that this exception regarding the threshold dpa was not due to a spatial variation of damage induced within the sample during the irradiation, the dpa was calculated per slice of depth of 1 nm along the thickness of the

sample using SRIM. If a section within the sample is subject to lower accumulation of damage, this specific section may prevent full amorphization until the necessary fluence is reached and thus result in a higher dpa threshold. However, when full amorphization was detected via the SADP, the section with the highest dpa in the krypton-irradiated sample was still lower than that of the xenon-irradiated sample, thus confirming that the observed lowest dpa threshold was not the result of spatial variation of the damage within the specimen. However, as the specimen irradiated with xenon was marginally thicker than the specimen irradiated with krypton ions, the irradiations were repeated under situations where the sample irradiated with xenon was thinner than that irradiated with krypton resulting in the same observation regarding the dpa threshold. It might be argue that the difference between the threshold dpa induced by the two ions is only slight, however, the simple fact that these threshold values are almost similar is, under these condition unlike what is usually anticipated in the literature, for both heterogeneous and homogeneous type of amorphization models. For instance, in [21], using experimental data and the critical damage energy density models (described in details in [17]), the authors concluded that at RT, the condition for amorphization of both germanium and silicon only depends in the nuclear energy transmitted to the target material regardless of the mass of the ion. As heavier ions (such as xenon ions compared to krypton ions) typically transfer more nuclear energy to the irradiated sample, a lower dpa threshold is thus usually observed.

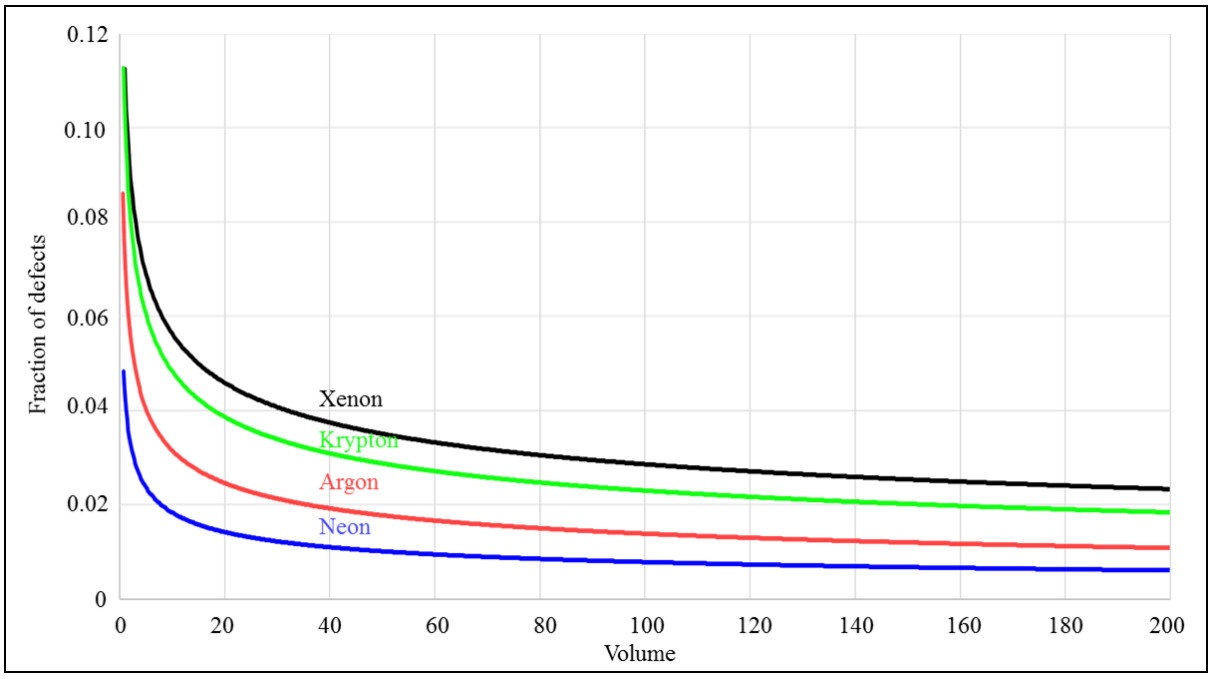

Figure 5. *Fraction of defects as a function of the cylindrical volume centred along the ion beam for each irradiation condition except for the specimen irradiated by helium ions.*

4.0 Discussion

As stated above, complete amorphization was achieved in all the irradiations performed for the current work and the evolution of the amorphous fraction indicates that a heterogeneous mechanism must be responsible for the amorphization process. Indeed, as described above and illustrated in figure 2, in a purely homogeneous mechanism, the f_a growth would have been expected to be more abrupt.[2], [3] However, even with the heaviest ion used here (xenon), a heterogeneous amorphization process based solely on the accumulation of amorphous pockets was not predicted, as V_d and $m \neq 0$. On the other hand, the presence of amorphous zones V_α induced by single-ion strikes has been identified even when the irradiation was performed by light ions such as neon (Z=10), thus showing that in most cases, the amorphization process must be expected to be a complex heterogeneous mechanism where both an amorphous region and a surrounding highly damaged shell both play a role in the build-up of the amorphous material.

Revealing the presence of amorphous zones in the collision cascades based on the recoil density calculations might seems arguable at first as SRIM does not take into account any dynamical effect which might lead to recombination of point defects, however, as the time scale under which the collapse of a crystalline region into an amorphous one is orders of magnitude lower than that required for thermal recombination or defects, the formation volume V_α can be assumed to be a reasonable estimate.[36]

Elsewhere,[1]–[3], [22] it has been observed that for matching average damage rate the efficiency (i.e. lower dpa threshold and value m, as well as larger values of V) associated with such a heterogeneous mechanism would increase with the mass of the incoming ions as they induce denser cascades.[2], [3] Most of these observations are in good agreement with the present work, however, as stated above and shown in table 1 the dpa threshold for amorphization of the specimen irradiated with xenon ions is not lower than for the specimen irradiated with krypton ions.

Being close in atomic mass, the nuclear energy transfer between krypton and germanium is more efficient than between xenon and germanium, leading to higher energy PKAs for a given ion energy. However, the overall nuclear energy transfer cannot by itself be responsible for the lower dpa threshold for krypton as the nuclear energy transferable to a germanium atom by a 300 keV xenon ion is higher than that from a 200 keV krypton ion by a factor of 1.4. The electronic energy loss may, (mainly) via bond rearrangement lower the final amount of damage caused by the nuclear loss. However, as shown in table 1 the calculated ratio S_e/S_n is larger for the krypton-irradiated sample than for the xenon-irradiated one, therefore, in this energy regime the electronic energy can reasonably be dismissed as responsible for the lower threshold dpa of krypton.

It is interesting to note that as reported previously in the literature, a heterogeneous mechanism would render invalid a direct proportionality between the number of point defects generated during irradiation and the rate of amorphization.[26] Indeed, MD simulations have shown that, with a heterogeneous mechanism, the fraction of defects generated within defect rich regions, (the regions *V*) were more likely to survive dynamic annealing and were the ones regulating the amorphization rate regardless of other point defects which may remain after dynamic annealing.[26] Consequently, it can be concluded that as the nature of the collision cascade differs from one ion to the other, the fraction of defects which mainly contribute to amorphization also differs. In other words, for a given ion there is necessarily a fraction of the atomic displacements that will not participate in amorphization and will therefore contribute to a rise of the dpa threshold. For light ions (such as neon) which are known to produce dilute collision cascades,[37] much of the damage will be generated outside the small highly damaged region which according to equation (2) is responsible for the amorphization build-up and can be approximated as having on average a volume (V_{Ne}= 40 nm^3). Whilst this mechanism seems to be justifying why typically, heavier ions are observed to have a lower dpa threshold, the comparison between xenon and krypton indicates otherwise as the dpa threshold of krypton is slightly lower than that of xenon.

Yet, the calculated volumes V and V_α for xenon and krypton cannot be responsible for the unexpected lower dpa threshold of krypton as V_{Xe} and $V_{\alpha\text{-}Xe}$ are bigger than V_{Kr} and $V_{\alpha\text{-}Kr}$. To better perceive how the threshold dpa should compare when irradiation is performed via different ions, it is important to

recall that the threshold dpa takes into account the overall number of displacements when amorphization has occurred, when in fact, a heterogeneous mechanism amorphization process depends on the displacements (or recoils) generated inside *V*. Thus, comparing the ratio of recoils within the volumes responsible for amorphization (V_α and *V*) with the overall number of recoils will indicate how the threshold dpa should compare. Indeed, ions which generate a bigger fraction of displacements outside the useful volume *V* should induce more "wasted" displacements and consequently should lead to a higher dpa threshold.

In figure 6(a), with the exception of the specimen irradiated by helium ions, are shown the fraction of displacements generated within the volume which becomes amorphous via single impact V_α and where dynamic annealing is thus disregarded. The figure clearly indicates that whilst there is a trend for heavier ions to have a greater percentage of their recoils within V_α, there is an exception when comparing the xenon-irradiated sample with the krypton-irradiated one.

As there are recoils within *V* which are also involved in the amorphization of germanium via the overlapping mechanism, the fraction of defects within *V* has also been calculated and is shown in figure 6 (b). Obviously, in this case the results are qualitative as all defects (or displacements) in the volumes *V* do not contribute to the amorphization process. Indeed, some will recombine via dynamic annealing. Yet, it is still remarkable that the same trend is observed, heavier ions induce a higher proportion of displacements within the defect cluster *V* than lighter ions, except, once more in the case of the specimen irradiated with krypton ions which has the highest proportion of recoils within *V*.

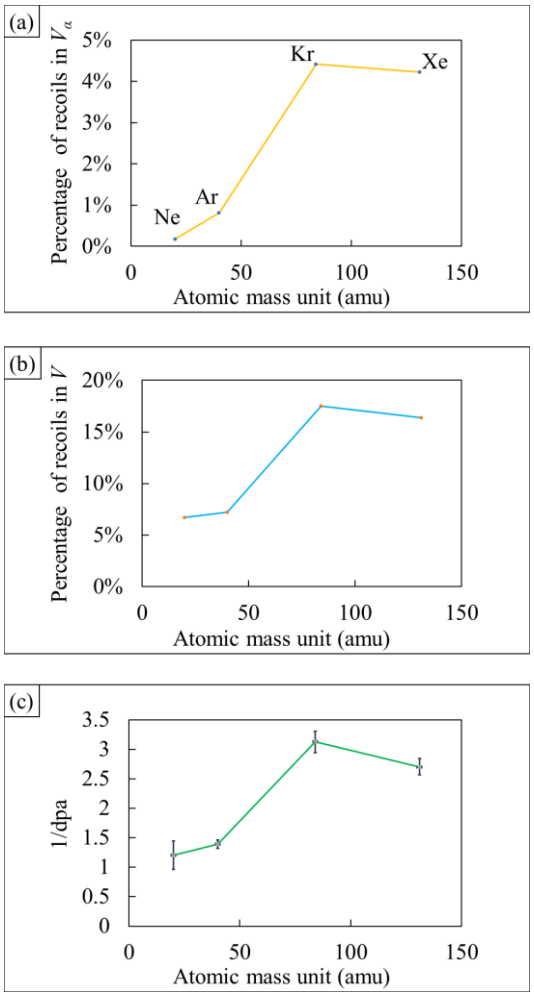

Figure 6. *Percentage of the recoils generated (a) within V_α and within (b) V as a function of the atomic mass unit in the case of the specimen irradiated by xenon (132 amu) krypton (84 amu) argon (40 amu) and neon (20 amu) ions. The inverse dpa is also shown (c) as a function of the atomic mass unit. The ion species indicated in (a) also applies for figures (b) and (c). The lines between the data points are just to guide the eye.*

The resemblance between the evolution of the dpa threshold as a function of the ion mass and the graphs of the fraction of defects within the volumes responsible for amorphization shown in figures 6(a)-(c) is indicative of the good agreement between the experimental results and calculated percentage of defects within V_α and V. They also illustrate that, whilst both xenon and krypton generate relatively dense cascades under this energy regime where the damage range is equivalent (i.e. about 80 nm in both case), the nature of their cascades is such that xenon generates a larger proportion of isolated defects compared with krypton thus resulting in a higher dpa threshold than for krypton. This counter-intuitive result is

another strong indication that highly damaged regions V_d and amorphous region V_α play a major role in the amorphization process, thus confirming a heterogeneous type of mechanism. Furthermore, it also shows that the dpa threshold for amorphization is an indicator that should be treated cautiously. Indeed, a low dpa threshold indicates only that a high proportion of displacements contribute to amorphization and can thus be misleading. In fact, it is worth noting that whilst the threshold dpa is lower in the krypton-irradiated specimen, the irradiation via the xenon ion was still able to amorphize the specimen more readily as amorphization has been achieved with a number of ions per unit volume (D) (i.e. fluence when amorphization occurred / thickness of the sample) that is 45 % lower under xenon ion irradiation than under Kr irradiation.

Irradiation with helium ions is often reported to be unable to induce complete amorphization of silicon and germanium at room temperature.[21] During irradiation by such a light ion most of the damage is dilute and the production of highly damaged regions of volume V are unlikely.[21], [26] The MC calculations show that on average a helium ion induces only 3 recoils in the 23 nm thick sample. However, as it will be shown here, the case of the specimen irradiated with helium is a typical example of how an average value does not reflect the stochastic nature of the collision cascades and can be misleading.

The analysis of 1000 cascades revealed that whilst 949 helium ions induced fewer than 10 recoils, 4 of them generated more than 100 recoils as well as clusters of defects and even amorphous regions whose volumes V_α can reach 65 nm^3 according to the defect density calculation made via the MATLAB code. The build-up of an amorphous layer via a heterogeneous mechanism can occur even if a few stable defect clusters are formed every 1000 ions but will necessarily require a higher fluence. Consequently, for the specimen irradiated by helium ions the stochastic nature of the collision cascades is of utmost importance as amorphization depends on collisions events which can be considered as rare (only 1 percent of the ions induce more than 50 recoils). It clarifies why amorphization is difficult to observe and only occurs at a fluence that is orders of magnitude higher than those of the heavier ions. Furthermore, it also explains why the threshold dpa is high as most of the displacements do not induce

clusters of defects but only point defects, which, in terms of a heterogeneous process can be considered essentially “useless” displacements for amorphization and thus contribute to a rise of the threshold dpa.

Lastly, equation (2) is used to determine *V* without taking into account that only a small fraction of the fluence participates in the heterogeneous process. There is therefore an overestimate of what can be termed the “effective fluence”, which, can be defined as the fraction of the dose which indeed generates a volume *V of defected material*. The calculation of *V* via the fluence instead of the useful fluence is the reason why the value of *V* as calculated by equation (2) is excessively small. Indeed, it gives an average value of what the volume of *V* would be if each helium ion were to generate a cluster of defects. This reasoning can be reasonably extended to the case of silicon, as recent work based on correlation between equation (2) and the evolution of SADPs during irradiation of silicon by 30 keV helium ions has also estimated an almost similar excessively small value for the volume *V* (0.13 nm^3).

5.0 Conclusion

By analysing SADPs taken over the course of ion irradiations of germanium, the dpa and the fluence threshold for amorphization of germanium under medium-energy inert-gas ions of masses ranging from 4 amu to 132 amu have been determined. These experiments should be useful to material scientists requiring a good estimate of the fluence needed to amorphize or to avoid amorphization of germanium at room temperature.

Using the correlation between the experimental results with both the equation relative to the overlapping model and the 3D analysis of the collision cascades, the build-up of amorphous layers was demonstrated to be the result of the accumulation of highly damaged regions whose core is amorphous. As expected, the number of overlaps needed for a cluster of defects to become amorphous tended to be higher when the ions were lighter, and the volume *V* of the damaged regions was bigger when the ions were heavier.

The unexpected case where the dpa threshold for amorphization was lower for krypton than xenon was demonstrated to be the result of the ability of a given ion to induce most of the atomic displacements in the form of highly damaged regions. It was found that there is a correlation between the threshold dpa for amorphization and the percentage of atomic displacements generated within highly damaged

regions. The role of defect clusters and amorphous pockets in the amorphization process was therefore confirmed to be crucial, corroborating a heterogeneous amorphization model.

For the specimen irradiated with helium ions, the average characteristics of the cascades indicate that the production of clusters of defects is a low probability event. However, the probability is not zero and the stochastic nature of the collision cascades ensures that a small proportion of helium ions can induce defect clusters and even amorphous regions. Consequently, the relatively high dpa threshold for amorphization and the small calculated volume V was concluded to be the due to the fact that only a fraction of fluence defined as the "effective fluence" was contributing to the amorphization mechanism.

Conflict of Interest

The authors declare no conflict of interest.

Acknowledgments

The authors are grateful to the EPSRC for financial support of this project (EP/M011135/1 and EP/M028283/1).

[1] L. Pelaz, L. A. Marqús, and J. Barbolla, "Ion-beam-induced amorphization and recrystallization in silicon," *J. Appl. Phys.*, vol. 96, no. 11, pp. 5947–5976, 2004.

[2] P. D. Edmondson *et al.*, "An in situ transmission electron microscopy study of the ion irradiation induced amorphisation of silicon by He and Xe," *Scr. Mater.*, vol. 113, pp. 190–193, 2016.

[3] P. D. Edmondson, D. J. Riley, R. C. Birtcher, and S. E. Donnelly, "Amorphization of crystalline Si due to heavy and light ion irradiation," *J. Appl. Phys.*, vol. 106, no. 4, pp. 1–8, 2009.

[4] L. A. Christel, J. F. Gibbons, and T. W. Sigmon, "Displacement criterion for amorphization of

silicon during ion implantation," *J. Appl. Phys.*, vol. 52, no. 12, pp. 7143–7146, 1981.

[5] A. Claverie, A. Roumili, N. Gessinn, and J. Beauvillain, "Kinetics of silicon amorphization by N+ implantation: Dose rate and substrate temperature effects," *Mater. Sci. Eng. B*, vol. 4, no. 1–4, pp. 205–209, Oct. 1989.

[6] J. S. Williams *et al.*, "Preferential amorphization and defect annihilation at nanocavities in silicon during ion irradiation," *Appl. Phys. Lett.*, vol. 77, no. 26, pp. 4280–4282, 2000.

[7] A. A. Lomov, A. V. Myakon'kikh, A. P. Oreshko, and A. A. Shemukhin, "Study of the amorphization of surface silicon layers implanted by low-energy helium ions," *Crystallogr. Reports*, vol. 61, no. 2, pp. 173–180, 2016.

[8] R. Mikšová, A. Macková, A. Jagerová, P. Malinský, P. Slepička, and V. Švorčík, "Structural study and ion-beam channelling in Si 〈1 0 0〉 modified by Kr+, Ag+, 2+and Au+, 2+ions," *Appl. Surf. Sci.*, vol. 458, no. July, pp. 722–733, 2018.

[9] J. Huang *et al.*, "Si amorphization by focused ion beam milling: Point defect model with dynamic BCA simulation and experimental validation," *Ultramicroscopy*, vol. 184, pp. 52–56, 2018.

[10] F. Priolo, T. Gregorkiewicz, M. Galli, and T. F. Krauss, "Silicon nanostructures for photonics and photovoltaics," *Nat. Nanotechnol.*, vol. 9, no. 1, pp. 19–32, 2014.

[11] D. Wang *et al.*, "Germanium nanowire field-effect transistors with SiO2 and high-κ HfO2 gate dielectrics," *Appl. Phys. Lett.*, vol. 83, no. 12, pp. 2432–2434, 2003.

[12] J. Greil, A. Lugstein, C. Zeiner, G. Strasser, and E. Bertagnolli, "Tuning the electro-optical properties of germanium nanowires by tensile strain," *Nano Lett.*, vol. 12, no. 12, pp. 6230–6234, 2012.

[13] J. R. Weber, A. Janotti, and C. G. Van de Walle, "Defects in Germanium," in *Photonics and Electronics with Germanium*, Weinheim, Germany: Wiley-VCH Verlag GmbH & Co. KGaA,

2015, pp. 1–23.

[14] H. Bracht, S. Schneider, and R. Kube, “Diffusion and doping issues in germanium,” *Microelectron. Eng.*, vol. 88, no. 4, pp. 452–457, 2011.

[15] H. Bracht, “Defect engineering in germanium,” *Phys. Status Solidi Appl. Mater. Sci.*, vol. 211, no. 1, pp. 109–117, 2014.

[16] A. Chroneos and H. Bracht, “Diffusion of n -type dopants in germanium,” *Appl. Phys. Rev.*, vol. 1, no. 1, 2014.

[17] G. Impellizzeri, S. Mirabella, and M. G. Grimaldi, “Ion implantation damage and crystalline-amorphous transition in Ge,” *Appl. Phys. A Mater. Sci. Process.*, vol. 103, no. 2, pp. 323–328, 2011.

[18] Jinning Liu, U. Jeong, M. Meloni, S. Mehta, and Che-Hoo Ng, “Effects of pre-amorphization on junction characteristics and damage behavior in low energy boron implantation,” in *2000 International Conference on Ion Implantation Technology Proceedings. Ion Implantation Technology - 2000 (Cat. No.00EX432)*, 2000, pp. 191–194.

[19] L. Capello *et al.*, “Influence of preamorphization on the structural properties of ultrashallow arsenic implants in silicon,” *J. Appl. Phys.*, vol. 100, no. 10, 2006.

[20] G. Velişa, E. Wendler, L.-L. Wang, Y. Zhang, and W. J. Weber, “Ion mass dependence of irradiation-induced damage accumulation in KTaO3,” *J. Mater. Sci.*, 2018.

[21] A. Claverie, S. Koffel, N. Cherkashin, G. Benassayag, and P. Scheiblin, “Amorphization, recrystallization and end of range defects in germanium,” *Thin Solid Films*, vol. 518, no. 9, pp. 2307–2313, 2010.

[22] J. F. Gibbons, “Ion implantation in semiconductors—Part II: Damage production and annealing,” *Proc. IEEE*, vol. 60, no. 9, pp. 1062–1096, 1972.

[23] L. A. Marqués, L. Pelaz, J. Hernández, J. Barbolla, and G. H. Gilmer, “Stability of defects in

crystalline silicon and their role in amorphization," *Phys. Rev. B - Condens. Matter Mater. Phys.*, vol. 64, no. 4, pp. 1–9, 2001.

[24] A. Rivera, J. Olivares, M. L. Crespillo, G. García, M. Bianconi, and F. Agulló-López, "Assessment of swift-ion damage by RBS/C: Determination of the amorphization threshold," *Nucl. Instruments Methods Phys. Res. Sect. B Beam Interact. with Mater. Atoms*, vol. 267, no. 8–9, pp. 1460–1463, May 2009.

[25] O. Peña-Rodríguez, J. Manzano-Santamaría, A. Rivera, G. García, J. Olivares, and F. Agulló-López, "Kinetics of amorphization induced by swift heavy ions in α-quartz," *J. Nucl. Mater.*, vol. 430, no. 1–3, pp. 125–131, Nov. 2012.

[26] M.-J. Caturla, T. Díaz de la Rubia, L. A. Marqués, and G. H. Gilmer, "Ion-beam processing of silicon at keV energies: A molecular-dynamics study," *Phys. Rev. B*, vol. 54, no. 23, pp. 16683–16695, 1996.

[27] J. F. Ziegler, M. D. Ziegler, and J. P. Biersack, "SRIM – The stopping and range of ions in matter (2010)," *Nucl. Instruments Methods Phys. Res. Sect. B Beam Interact. with Mater. Atoms*, vol. 268, no. 11–12, pp. 1818–1823, Jun. 2010.

[28] C. W. Lee, Y. Ikematsu, and D. Shindo, "Measurement of mean free paths for inelastic electron scattering of Si and SiO2," *J. Electron Microsc. (Tokyo).*, vol. 51, no. 3, pp. 143–148, 2002.

[29] P. D. Edmondson *et al.*, "An in situ transmission electron microscopy study of the ion irradiation induced amorphisation of silicon by He and Xe," *Scr. Mater.*, vol. 113, pp. 190–193, 2016.

[30] I. Jenčič, M. W. Bench, I. M. Robertson, and M. A. Kirk, "Electron- beam- induced crystallization of isolated amorphous regions in Si, Ge, GaP, and GaAs," *J. Appl. Phys.*, vol. 78, no. 2, pp. 974–982, Jul. 1995.

[31] I. Jenčič and I. . Robertson, "Regrowth of heavy-ion implantation damage by electron beams,"

Mater. Sci. Semicond. Process., vol. 3, no. 4, pp. 311–315, Aug. 2000.

[32] C. A. Schneider, W. S. Rasband, K. W. Eliceiri, and C. Instrumentation, "NIH Image to ImageJ: 25 years of Image Analysis HHS Public Access," *Nat. Methods*, vol. 9, no. 7, pp. 671–675, 2012.

[33] O. Camara *et al.*, "Shape Modification of Germanium Nanowires during Ion Irradiation and Subsequent Solid-Phase Epitaxial Growth," *Adv. Mater. Interfaces*, vol. 5, no. 13, p. 1800276, Jul. 2018.

[34] E. Holmström, K. Nordlund, and A. Kuronen, "Threshold defect production in germanium determined by density functional theory molecular dynamics simulations," *Phys. Scr.*, vol. 81, no. 3, p. 035601, Mar. 2010.

[35] M. L. Swanson, J. R. Parsons, and C. W. Hoelke, "Damaged regions in neutron-irradiated and ion-bombarded Ge and Si," *Radiat. Eff.*, vol. 9, no. 3–4, pp. 249–256, Jun. 1971.

[36] W. P. Maszara and G. A. Rozgonyi, "Kinetics of damage production in silicon during self-implantation," *J. Appl. Phys.*, vol. 60, no. 7, pp. 2310–2315, 1986.

[37] H. H. Andersen and H. L. Bay, "Heavy- ion sputtering yields of gold: Further evidence of nonlinear effects," *J. Appl. Phys.*, vol. 46, no. 6, pp. 2416–2422, Jun. 1975.